Angular Momentum-Dependent Transmission of Circularly Polarized Vortex Beams Through a Plasmonic Coaxial Nanoring
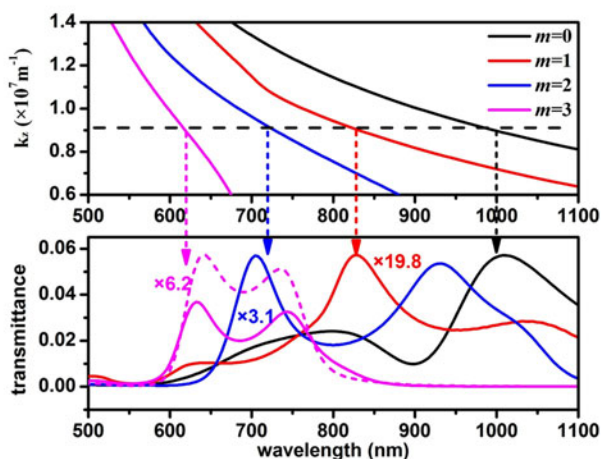
Shuai Wang
Zi-Lan Deng
Yaoyu Cao
Dejiao Hu
Yi Xu
Boyuan Cai
Long Jin
Yuan Bao
Xiaolei Wang
Xiangping Li

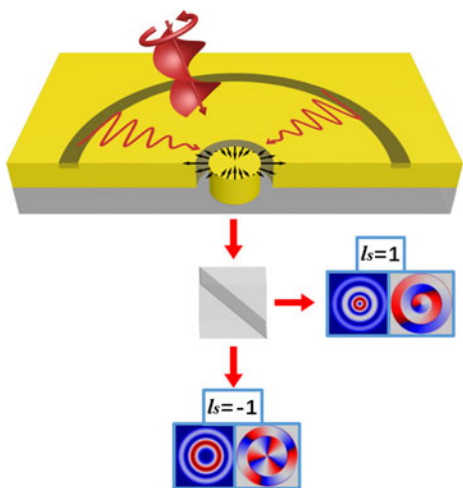# Angular Momentum-Dependent Transmission of Circularly Polarized Vortex Beams Through a Plasmonic Coaxial Nanoring

Shuai Wang,[1,2] **Zi-Lan Deng** ⓘ**,**[2] **Yaoyu Cao,**[2] **Dejiao Hu,**[2] **Yi Xu,**[2]
Boyuan Cai,[3] **Long Jin** ⓘ**,**[2] **Yuan Bao,**[2] **Xiaolei Wang,**[1]
and Xiangping Li ⓘ [2]

[1]Institute of Modern Optics, Key Laboratory of Optical Information Science and Technology,
Nankai University, Tianjin 300350, China
[2]Guangdong Provincial Key Laboratory of Optical Fiber Sensing and Communications,
Institute of Photonics Technology, Jinan University, Guangzhou 510632, China
[3]Nanophotonics, Shenzhen University, Shenzhen 518060, China

Abstract: In this paper, we report on the theoretical and numerical study of the transmission of circularly polarized vortex beams through a plasmonic coaxial nanoring. We show that the transmission peak wavelength of an incident circularly polarized vortex beam is dominantly governed by the total angular momentum, which determines the coupling to the plasmonic eigenmode supported by the coaxial nanoring with a given geometry and ultimately the transmitted beam in the far field. In addition, our study shows that the total angular momentum of the incident circularly polarized vortex beam can be conserved, where the far field of the transmitted beam contains both left- and right-handed circular polarization components with correspondingly modulated orbital angular momentum preserving the same total angular momentum. Our work can be potentially useful to advanced nanophotonic devices harnessing light's angular momentum division.

Index Terms: Surface plasmons, optical vortices, micro-optical devices.

1. Introduction

As one of the most fundamental physical properties in both classical and quantum optics, angular momentum (AM) including both spin angular momentum (SAM) carried by circularly polarized photons and orbital angular momentum (OAM) associated with the helical wavefront of light [1] has mediated many appealing applications, such as optical communications, super-resolution imaging, optical tweezing and so on [2]–[6]. The total AM carried by a beam generally expressed as $L = l_s + l_o$ usually plays crucial roles, where the SAM $l_s = \pm 1$ represents left- and right-handed circular (LHC/RHC) polarization, respectively, and the OAM taking arbitrary integer values ($l_o = 0 \pm 1, \pm 2 \ldots$) manifests multiple cycles of phase changes. In particular, its physically-orthogonal nature has enabled onrushing developments of employing light's AM state as a new
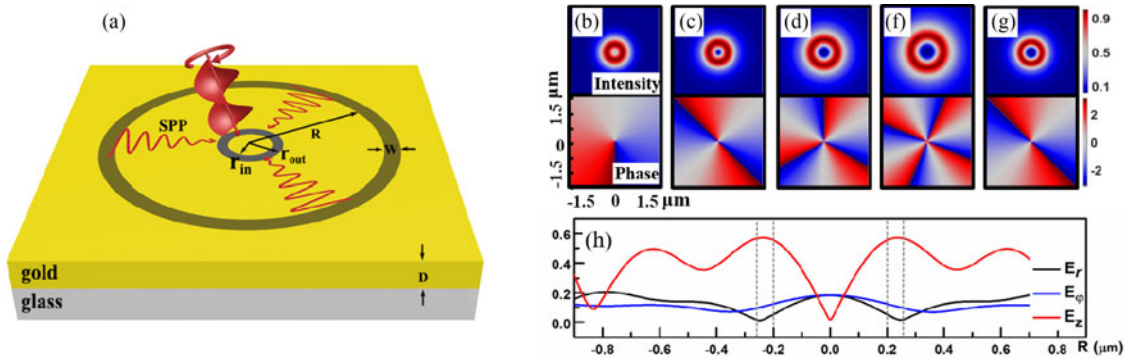
Fig. 1. (a) Schematic of the plasmonic coaxial nanoring with an inner radius of r_{in} and an outer radius r_{out} enclosed by a concentric nano-groove with an inner radius R, a width of W, and a thickness of D. (b) to (g) show the intensity and phase distribution of the incident beams of RHC polarization with OAM of 1, 2, 3, 4 ($l_s = -1$, $l_o = 1, 2, 3, 4$) and LHC polarization with OAM of 2 ($l_s = 1$, $l_o = 2$). (h) Comparison of the three field components of the SPP mode excited at the top surface by the incident beam with a total AM of 1 ($l_s = -1$, $l_o = 2$), the gray dashed lines symbol the position of the nanoring slit.

multiplexing division for high-capacity optical information technologies from free space [7] to compact nanophotonic devices [8].

In this regard, surface plasmon structures capable of deep light confinement at the nanoscale emerge as new approaches toward miniaturized optical devices harnessing light's AM division [9]–[12]. Beams carrying predesigned AM states can be generated by passing through plasmonic nano-antennas arranged on chip-scale planar optics [13]. Later, it has been demonstrated that plasmonic nano-apertures such as nano-slits [11], [14], [15] and nano-gratings [16] can be employed to separate not only SAM but also OAM states into different propagating directions. In general, light's interaction with plasmonic subwavelength antennas or apertures can be well described by a transmission process of the linear momentum of light, where incoming photons couple to surface plasmons, which tunnel through the subwavelength structure and then convert back to photons through the wavevector matching [17], [18]. The transmission of the circularly polarized vortex beams through plasmonic coaxial nanoring has been long overlooked, although the insight could provide new perspectives for advanced nanophotonic devices based on the manipulation of light's AM state.

Owing to their cylindrical symmetry, plasmonic coaxial nano-apertures have been intensely investigated for linear momentum dependent transmission [19]–[25]. In this paper, the transmission of circularly polarized vortex beams through a plasmonic coaxial nanoring is systematically investigated both theoretically and numerically, which exhibits unique AM dependent transmission for nanoscale AM multiplexing [8], [26].

2. Angular Momentum Dependent Transmission

The schematic illustration of the plasmonic coaxial nanoring under investigation is shown in Fig. 1(a). A coaxial nanoring prepared on the glass substrate with an inner radius $r_{in} = 200$ nm and an outer radius $r_{out} = 250$ nm is concentrically enclosed by a nano-groove with an inner radius $R = 1\,\mu$m, a width $W = 100$ nm and a depth $d = 100$ nm. The metal is chosen as gold with a thickness of $D = 200$ nm, and the permittivity of gold is taken from the Johnson and Christy's paper [27]. Without loss of generality, Fig. 1(b)–(g) depict examples of the intensity and phase distribution of the incident beams of RHC polarization with OAM of 1, 2, 3, 4 ($l_s = -1$, $l_o = 1, 2, 3, 4$) and LHC polarization with OAM of 2 ($l_s = 1$, $l_o = 2$), where the focal field is obtained by an objective lens with numerical aperture 0.4 at the wavelength of 500 nm.
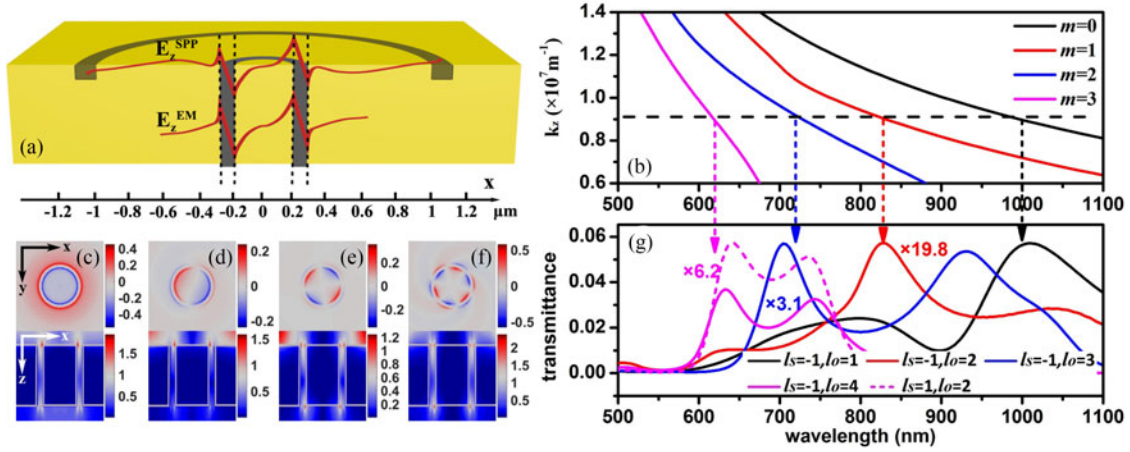
Fig. 2. (a) Illustration of the transmission process determined by the coupling between the SPP mode launched by the nano-groove and the CSP eigenmode supported in the coaxial nanoring. (b) The real part of the propagation constant (k_z) of the first four CSP modes with AM $m = 0, 1, 2, 3$. The dashed line indicates the first order longitudinal resonance, where the end facets shift the resonant phase from π to 0.582π by considering the finite thickness of the plasmonic waveguide. (c) to (f) Simulated electric fields in the transverse and longitudinal planes for the four CSP modes with AM $L = 0, 1, 2, 3$ ($l_s = -1$, $l_o = 1, 2, 3, 4$) at the resonant wavelength of 1007 nm, 830 nm, 705 nm and 634 nm, respectively. (g) Simulated transmission spectra of the incident circularly polarized beams with total AM $L = 0, 1, 2, 3$.

The concentric nano-groove is responsible for efficiently converting AM beams to the SPP and concentrates the SPP to the center of the nanoring [28], [29]. The z-component of electric fields is clearly dominant in the SPP mode compared with transverse components, as illustrated in Fig. 1(h). Due to the fact that only the radial component of the electric fields of incident beams can efficiently excite the SPP, the dominant z-component of electric fields of the plasmonic mode at the observation point (R, θ) can be written as [8]:

$$E_z^{spp}(R, \theta) \sim C_1^L e^{iL\varphi} e^{-k_{spp,z}z} JL(k_{spp,r}R) \tag{1}$$

where $L = l_s + l_o$ represents the total AM carried by the incident beam [30], J_L is the L th order Bessel function of the first kind and C_1^L represents the coupling coefficient from the free space wave to the SPP. It reveals clearly that the launched SPP carries the same total AM inherited from the incident circularly polarized vortex beam.

According to the coupled-mode theory, the overall transmittance is mainly determined by the coupling between the SPP mode launched by the nano-groove and the eigenmode supported in the coaxial nanoring. As an example, the SPP mode with the total AM $L = 1$ ($l_s = -1$, $l_o = 2$) carried by the incident RHC beam and the eigenmode supported in the nanoring are shown in Fig. 2(a). The coupling coefficient C_2^L from the SPP mode to the cylindrical surface plasmon (CSP) eigenmode is defined as:

$$C_2^L \sim \int_0^{2\pi} d\varphi \int_0^{+\infty} \frac{E_z^{L\,spp} \cdot E_z^{L\,em}}{\left|E_z^{L\,spp}\right|\left|E_z^{L\,em}\right|} dr \tag{2}$$

where $E_z^{L\,spp}$ is the z-component of the electric fields of the SPP mode launched by the nano-groove, $E_z^{L\,em}$ is the z-component of the electric fields of the eigenmode supported by the nanoring. To get an insight into the transmission process of AM carrying beams through the plasmonic coaxial nanoring, our theoretical model consists of an infinite long coaxial waveguide supporting the CSP [20]. In general, all field components of supported eigenmodes can be expressed in terms of the TM and TE wave functions, and their first and second derivatives with respect to the cylindrical

coordinates, in the three geometrical domains (gold core, air gap and gold cladding) [8]:

$$E_z^m = \exp\left(im\varphi\right)\exp\left(i\,k_z\,z\right) \begin{cases} A_1\,I_m\left(k_1 r\right) & \text{gold core} \\ A_2\,I_m\left(k_2 r\right) + A_3\,K_m\left(k_2 r\right) & \text{air gap} \\ A_4\,K_m\left(k_1 r\right) & \text{gold cladding} \end{cases} \tag{3}$$

$$H_z^m = \exp\left(im\varphi\right)\exp\left(i\,k_z\,z\right) \begin{cases} B_1\,I_m\left(k_1 r\right) & \text{gold core} \\ B_2\,I_m\left(k_2 r\right) + B_3\,K_m\left(k_2 r\right) & \text{air gap} \\ B_4\,K_m\left(k_1 r\right) & \text{gold cladding} \end{cases} \tag{4}$$

$$E_r = -\frac{i}{k_i^2}\left(k_z \frac{\partial E_z^m}{\partial r} + w u_0 \frac{1}{r}\frac{\partial H_z^m}{\partial \varphi}\right) \tag{5}$$

$$E_\varphi = -\frac{i}{k_i^2}\left(k_z \frac{1}{r}\frac{\partial E_z^m}{\partial \varphi} - w u_0 \frac{\partial H_z^m}{\partial r}\right) \tag{6}$$

$$H_r = -\frac{i}{k_i^2}\left(k_z \frac{\partial H_z^m}{\partial r} - w \varepsilon_i \frac{1}{r}\frac{\partial E_z^m}{\partial \varphi}\right) \tag{7}$$

$$H_\varphi = -\frac{i}{k_i^2}\left(k_z \frac{1}{r}\frac{\partial H_z^m}{\partial \varphi} + w \varepsilon_i \frac{\partial E_z^m}{\partial r}\right) \tag{8}$$

where m is mth order AM mode of the coaxial nanoring, k_z is longitudinal wavenumber, I and K are modified Bessel functions of the first and second kind, respectively. k_i ($i = 1, 2$) are transverse wave numbers in the gold core and cladding or air, respectively, ω is the angular frequency, μ_0 is the permeability constant, ε_i is the permittivity of gold or air, respectively, and A and B are the unknown coefficients. Fig. 2(b) shows the dispersion curves of eigenmodes of the coaxial nanoring obtained by solving the matrix satisfying the boundary conditions at both inner and outer interfaces. The real parts of the propagating constant (k_z) of the first four modes with AM $m = 0, 1, 2, 3$ are graphed as functions of the wavelength.

It is intuitive to understand that the SPP carrying AM inherited from the incident circularly polarized vortex beam can tunnel through the coaxial nanoring as long as the SPP mode matches an eigenmode with an identical AM in the nanoring [31]. In addition, the transmittance exhibits a peak when the longitudinal resonance supported by the nanoring with a given length is reached as

$$k_z D = n\pi + \phi \tag{9}$$

where n is the longitudinal mode number. Since our theoretical model assumes an infinite length of the coaxial nanoring, a phase shift ϕ is introduced to count the interference effect from the end facets [32]. In Fig. 2(b), the intersections of the dashed line with the dispersion curves give the wavelength at which the CSP mode is at resonance with the longitudinal mode ($n = 1$), and hence the transmittance exhibits a peak there. Then, the excited CSP mode at the exit facet can couple out to free space waves and diffract to the far field, allowing the total AM dependent transmission.

The full wave simulation by finite-difference time-domain (FDTD) methods bears out the above modal analysis. Fig. 2(g) shows the transmission spectra of the incident circularly polarized vortex beam with a total AM $L = 0, 1, 2, 3$ ($l_s = -1$, $l_o = 1, 2, 3, 4$ and $l_s = 1$, $l_o = 2$). The arrows indicate the transmission peak wavelengths surmised by the modal analysis with a fitted phase shift of $\phi = -1.314$. A reasonable correspondence between the resonant wavelengths in the simulations in Fig. 2(g) with those obtained with the dispersion curves with the resonance condition of Eq. (9) is observed. It should be noted that the peaks at the longer wavelengths in CSP modes with $m = 2$ and 3 represent the longitudinal mode at the resonance order n = 0 [33]. Fig. 2(c)–(f) show the simulated electric fields for the four incident beams with total AM $L = 0, 1, 2, 3$ ($l_s = -1$, $l_o = 1, 2, 3, 4$) at the resonant wavelengths. The top and bottom panels show the field E_z and intensity distribution in the transverse and longitudinal planes, respectively. The deterministic mode distribution in both transverse and longitudinal planes clearly verifies the AM of the CSP mode and the longitudinal mode resonance. For those incident beams with different SAM and OAM, but the same total AM

$L = 3$ ($l_s = -1$, $l_o = 4$ and $l_s = 1$, $l_o = 2$), the transmission behaviors are similar [magenta solid and dashed curves in Fig. 2(g)], except that the transmitted intensities vary slightly. By taking the coupling coefficients in the transmission process into consideration, the simulation reveals absolute transmittances of the nanoring with the given geometry to be 0.057, 0.0029, 0.018, 0.0059 for those incident beams with total AM $L = 0, 1, 2, 3$ ($l_s = -1$, $l_o = 1, 2, 3, 4$) at the peak wavelength of 1007 nm, 830 nm, 705 nm and 634 nm, respectively. It clearly demonstrates that the transmission peak wavelength depends on the total AM of the incident beam, which provides a facile way to select the transmission wavelength by the combination of the spin and orbital AM carried by the incident beam.

Although the transmission peak wavelength can be easily determined by the total AM of the incident beam, the overall transmittance can be tuned by a series of parameters such as the depth of the nano-groove, the geometry of the nanoring, the incident field's distribution and the absorption losses in the gold film and so on. The conversion efficiency from the incident beam to the SPP mode can be changed by adjusting the depth of the nano-groove, hence affecting the transmission. The propagation constant curve will have a red shift when increasing the radius of the nanoring according to Eqs. (3)–(8), the wavelength of the transmission peak will have a correspondent shift due to the mode-matching condition. The transmission peak wavelength can be further tuned by varying the length of the nanoring, the thickness of the gold layer, to shift the longitudinal resonance according to Eq. (9). For a given longitudinal mode, the real part of the propagation constant (k_z) is inversely proportional to the length of the nanoring. As a result, increasing the length of nanoring leads to the red shift of the transmission peak. From Eqs. (3)–(8), we see that the eigenmodes supported by the nanoring also depend on the slit width of the nanoring. We further investigate the influence of the slit width of the nanoring by rigorous full wave simulations. Fig. 3(a)–(d) show the simulated normalized transmittance of incident beams with total AM $L = 0, 1, 2, 3$ ($l_s = -1$, $l_o = 1, 2, 3, 4$) by adjusting the outer radius of nanorings from 230 nm to 300 nm while keeping the inner radius at 200 nm, corresponding to an increase of the slit width from 30 to 100 nm. It can be seen that the increasing of the slit width of the nanoring can enhance the transmission peak value as well as the bandwidth of the transmission peak, which is due to the increased coupling of the nanoring with the incident free space light and the decreased quality factor of the resonance mode. The variation of transmission peak value upon the width of the nanoring provides a pathway to obtain uniform transmittance for different incident beams.

The interaction between nano-groove and incident beams with different beam size can affect the launched SPP intensity, and thus influence the overall transmittance. The intensity distribution of the incident field ($l_s = -1$, $l_o = 3$) along the radial direction and the full width at half maximum of those beams are shown in the inset and legend of Fig. 4(a), respectively. It reveals clearly that increasing the beam size leads to the decrease of the transmittance peak value without any variation of peak wavelengths, which is a result of the decreased coupling efficiency from the free space wave to the SPP. In addition, the appearance of dissipative losses in the gold film can also lead to a decreased absolute transmittance, which mainly stems from the propagation loss of the CSP mode in the nanoring by considering the metallic absorption. This is in particular for higher order AM CSP modes that generally exhibit higher propagation losses [34], as evidenced in Fig. 4(b). The comparison of the overall transmittance with and without the losses in the gold film shows a significantly increased transmittance reduction from 77% to 26% for the incident beams with the total AM $L = 0, 1, 2, 3$ ($l_s = -1$, $l_o = 1, 2, 3, 4$) at the resonant wavelength of 1007 nm, 830 nm, 705 nm and 634 nm, respectively.

3. Evolution of Angular Momentum

The evolution of the AM state of circularly polarized vortex beams during the transmission process can be obtained by the field analysis of the transmitted beam from the coaxial nanoring. The calculation by Eqs. (3)–(8) reveals that the transverse electric field component E_r of the eigenmode is dominant at the exit facet of the nanoring. Fig. 5 depicts the calculated E_r distribution for the four CSP modes with the AM $L = 0, 1, 2, 3$ at the corresponding resonant wavelengths, respectively. Owing
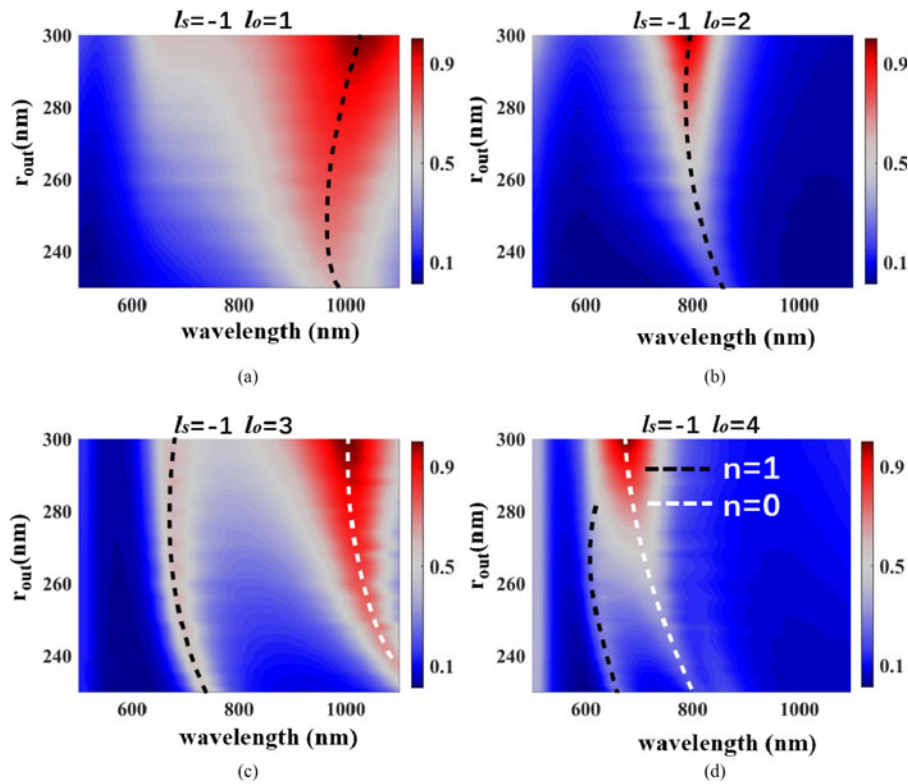
Fig. 3. The normalized transmittance of different circularly polarized vortex beams (a) $l_s = -1$, $l_o = 1$, (b) $l_s = -1$, $l_o = 2$, (c) $l_s = -1$, $l_o = 3$, (d) $l_s = -1$, $l_o = 4$, as a function of the wavelength and the outer radius of the nanoring. The black and white dash curves present the first and zeroth longitudinal resonance order along the z-direction, respectively.
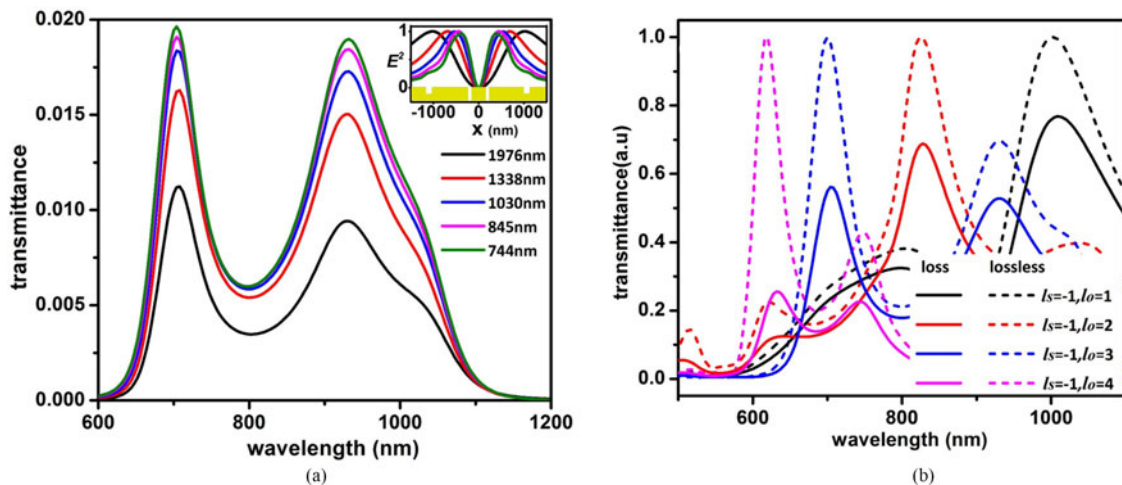

Fig. 4. (a) The transmittance of incident beams carrying the same SAM and OAM ($l_s = -1$, $l_o = 3$), but with different beam waists as shown in the inset and legend. (b) The transmittance of different incident circularly polarized vortex beams with (solid) and without (dashed) losses in the gold film.
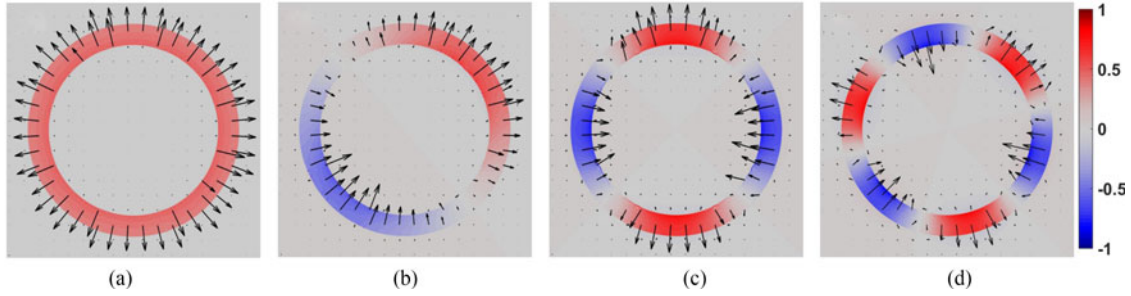
Fig. 5. (a) to (d) The dominant transverse electric-field components of the four CSP eigenmodes of AM = 0, 1, 2, 3 at the corresponding resonant wavelength of 1007 nm, 830 nm, 705 nm and 634 nm, respectively.

to the cylindrical symmetry, they exhibit features of radially polarized vortex beams superposed with a topological charge L equal to the total AM of the incident circularly polarized vortex beams. Such vortex beams at the exit facet can be generally described in a circular basis [35]

$$E(r, \varphi) = E_0(r) \left\{ \frac{1}{\sqrt{2}} \exp\left[i(L-1)\varphi\right] \right\} |LHC\rangle + E_0(r) \left\{ \frac{1}{\sqrt{2}} \exp\left[i(L+1)\varphi\right] \right\} |RHC\rangle \quad (10)$$

where $E_0(r)$ is the radial field distribution that can be derived by Eqs. (3)–(8), the far field transmitted beam can be treated as the Fraunhofer diffraction of the transmitted field

$$E(r, \varphi, z) \sim C_3^L \frac{k \exp(ikz)}{\sqrt{2}z} \left\langle \left\{ \exp\left[i(L-1)\varphi\right] \int_0^{+\infty} E_0(r') J_{L-1}\left(\frac{krr'}{z}\right) r' dr' \right\} |LHC\rangle \right.$$

$$\left. + \left\{ \exp\left[i(L+1)\varphi\right] \int_0^{+\infty} E_0(r') J_{L+1}\left(\frac{krr'}{z}\right) r' dr' \right\} |RHC\rangle \right) \quad (11)$$

where, k is the wavenumber, z is the propagate distance, C_3^L is the out-coupling coefficient from the CSP mode to the free space wave through the nanoring. As speculated from Eq. (11), the far field transmitted beam can be decomposed into LHC and RHC components superposed with a topological charge of $L - 1$ and $L + 1$, respectively. It reveals clearly that the total AM of the incident circularly polarized vortex beam can be conserved, where the transmitted beam contains both LHC and RHC components with correspondingly modulated OAM preserving the same total AM. Thus, the AM conservation law is generally obeyed during the transmission process.

The theoretical analysis is verified by the FDTD simulation as shown in Fig. 6. The transmitted beam at the exit facet is projected to the far field and analyzed in LHC and RHC polarization components carrying an identical energy, as illustrated in Fig. 6(a). Fig. 6(b) presents the far field LHC and RHC components when the incident beam is LHC ($l_s = 1$) superposed with OAM $l_o = 0, 1, 2$. Indeed, from the intensity and phase distribution it unambiguously reveals that the transmitted beams conserve the total AM of incident circularly polarized vortex beams. Out-coupled LHC polarization beams conserve both SAM and OAM consistent with the LHC incident beams, while the out-coupled RHC polarization beams with an augmented topological charge by 2. When the incident beam is switched to the RHC polarization with different OAM, similar tendency with conserved SAM and OAM in the RHC polarization while the LHC polarization with a decreased OAM by 2 is observed in Fig. 6(c). Our numerical result is consistent with the theoretical analysis. Thus, the transmission law of light's AM through a plasmonic coaxial nanoring is demonstrated.

It should be noted that the transmittance is complicated when a linearly polarized vortex beam is taken as the incident beam. For radial polarization vortex beams, they can be decomposed into RHC and LHC components, each of which generally conserves the total AM during the transmission process, although the absolute transmittance varies significantly due to the total AM dependent transmission peaks for different circular polarization components. However, for linear and azimuthal
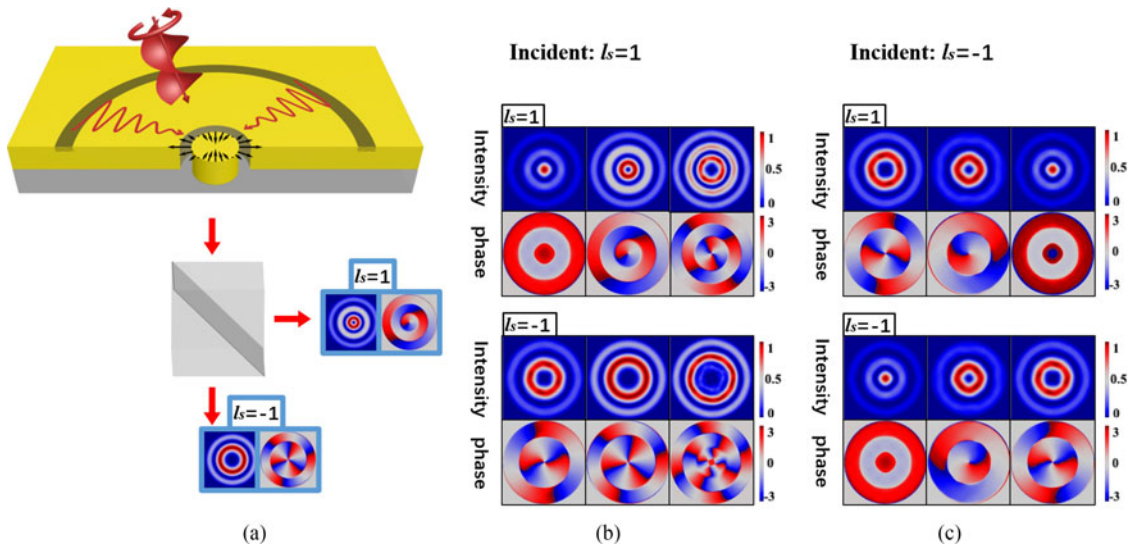
Fig. 6. (a) Illustration of the analysis of the transmitted beam in LHC ($l_s = 1$) and RHC ($l_s = -1$) polarization components, respectively. (b) and (c) show the far field intensity and phase of LHC and RHC components when the incident beam is (b) LHC and (c) RHC with OAM $l_o = 0$, 1, 2, respectively.

polarization beams, the SPP mode at the upper surface of nanoring cannot be efficiently excited, neither the subsequent coupling nor transmission processes are valid any more.

4. Conclusion

In conclusion, we have investigated the transmission of circularly polarized vortex beams through a plasmonic coaxial nanoring both theoretically and numerically. The transmission of a plasmonic coaxial nanoring with a given geometry can be selectively tuned upon the total AM carried by the incident beam. The transmission peak appears when the total AM of the incident circularly polarized vortex beam matches that of the CSP eigenmode supported in the plasmonic coaxial nanoring, which is in resonance with the longitudinal mode along its length direction. The parametric influence on the overall transmittance including the depth of the nano-groove, the width of the slit, the width of the incident beam and metallic losses has been discussed. In addition, our study reveals that the total AM is conserved during the transmission process. The far field of the transmitted beam stemming from the out-coupling of the CSP eigenmode containing both LHC and RHC components where one circular polarization component congruent with the incident circular polarization beam preserves the OAM while a concomitant polarization exhibits opposite SAM supposed with correspondingly altered OAM. The underlying insight into the transmission of circularly polarized vortex beams in nano-structures provides a scientific and technological basis for advanced nanophotonic applications harnessing the AM division such as multiplexed optical communication [8], [36] and data storage [37].

References

[1] A. T. O'Neil, I. MacVicar, L. Allen, and M. J. Padgett, "Intrinsic and extrinsic nature of the orbital angular momentum of a light beam," *Phys. Rev. Lett.*, vol. 88, no. 5, Jan. 16, 2002, Art. no. 053601.

[2] G. Gibson *et al.*, "Free-space information transfer using light beams carrying orbital angular momentum," *Opt. Exp.*, vol. 12, no. 22, pp. 5448–5456, 2004.

[3] A. Liu, G. Rui, X. Ren, Q. Zhan, G. Guo, and G. Guo, "Encoding photonic angular momentum information onto surface plasmon paritons with plasmonic lens," *Opt. Exp.*, vol. 20, no. 22, pp. 24151–24159, 2012.

[4] L. Li and F. Li, "Beating the Rayleigh limit: Orbital-angular-momentum-based super-resolution diffraction tomography," *Phys. Rev. E*, vol. 88, no. 3, 2013, Art. no. 033205.

[5] W.-Y. Tsai, J.-S. Huang, and C.-B. Huang, "Selective trapping or rotation of isotropic dielectric microparticles by optical near field in a plasmonic Archimedes spiral," *Nano Lett.*, vol. 14, no. 2, pp. 547–552, 2014.

[6] X. Li, P. Venugopalan, H. Ren, M. Hong, and M. Gu, "Super-resolved pure-transverse focal fields with an enhanced energy density through focus of an azimuthally polarized first-order vortex beam," *Opt. Lett.*, vol. 39, no. 20, pp. 5961–5964, 2014.

[7] J. Wang *et al.*, "Terabit free-space data transmission employing orbital angular momentum multiplexing," *Nature Photon.*, vol. 6, no. 7, pp. 488–496, 2012, doi: 10.1038/nphoton.2012.138.

[8] H. Ren, X. Li, Q. Zhang, and M. Gu, "On-chip noninterference angular momentum multiplexing of broadband light," *Science*, vol. 352, no. 6287, pp. 805–809, 2016.

[9] S. Yang, W. Chen, R. L. Nelson, and Q. Zhan, "Miniature circular polarization analyzer with spiral plasmonic lens," *Opt. Lett.*, vol. 34, no. 20, pp. 3047–3049, 2009.

[10] G. Rui, W. Chen, and Q. Zhan, "High efficiency plasmonic probe design for parallel near-field optics applications," *Opt. Exp.*, vol. 19, no. 6, pp. 5187–5195, 2011.

[11] Y. Li *et al.*, "Orbital angular momentum multiplexing and demultiplexing by a single metasurface," *Adv. Opt. Mater.*, vol. 5, no. 2, 2017, Art. no. 1600502.

[12] M. Pu *et al.*, "Spatially and spectrally engineered spin-orbit interaction for achromatic virtual shaping," *Sci. Rep.*, vol. 5, 2015, Art. no. 9822.

[13] G. Rui, R. L. Nelson, and Q. Zhan, "Beaming photons with spin and orbital angular momentum via a dipole-coupled plasmonic spiral antenna," *Opt. Exp.*, vol. 20, no. 17, pp. 18819–18826, 2012.

[14] J. Lin *et al.*, "Polarization-controlled tunable directional coupling of surface plasmon polaritons," *Science*, vol. 340, no. 6130, pp. 331–334, 2013.

[15] L. Huang *et al.*, "Helicity dependent directional surface plasmon polariton excitation using a metasurface with interfacial phase discontinuity," *Light Sci. Appl.*, vol. 2, p. e70, 2013.

[16] P. Genevet, J. Lin, M. A. Kats, and F. Capasso, "Holographic detection of the orbital angular momentum of light with plasmonic photodiodes," *Nature Commun.*, vol. 3, 2012, Art. no. 1278.

[17] T. W. Ebbesen, H. J. Lezec, H. F. Ghaemi, T. Thio, and P. A. Wolff, "Extraordinary optical transmission through sub-wavelength hole arrays," *Nature*, vol. 391, no. 6668, pp. 667–669, 1998, doi: 10.1038/35570.

[18] T. Li *et al.*, "Manipulating optical rotation in extraordinary transmission by hybrid plasmonic excitations," *Appl. Phys. Lett.*, vol. 93, no. 2, 2008, Art. no. 021110.

[19] H. Marie Anne van de, M. Ruben, B. Benjamin, and P. Albert, "Surface plasmon polariton modes in coaxial metal-dielectric-metal waveguides," *New J. Phys.*, vol. 18, no. 4, 2016, Art. no. 043016.

[20] M. I. Haftel, C. Schlockermann, and G. Blumberg, "Enhanced transmission with coaxial nanoapertures: Role of cylindrical surface plasmons," *Phys. Rev. B*, vol. 74, no. 23, 2006, Art. no. 235405.

[21] N. Shitrit, S. Nechayev, V. Kleiner, and E. Hasman, "Spin-dependent plasmonics based on interfering topological defects," *Nano Lett.*, vol. 12, no. 3, pp. 1620–1623, 2012.

[22] N. Tischler *et al.*, "Experimental control of optical helicity in nanophotonics," *Light Sci. Appl.*, vol. 3, p. e183, 2014.

[23] X. Zambrana-Puyalto, X. Vidal, I. Fernandez-Corbaton, and G. Molina-Terriza, "Far-field measurements of vortex beams interacting with nanoholes," *Sci. Rep.*, vol. 6, 2016, Art. no. 22185.

[24] X.-F. Ren, G.-P. Guo, Y.-F. Huang, Z.-W. Wang, and G.-C. Guo, "Spatial mode properties of plasmon-assisted transmission," *Opt. Lett.*, vol. 31, no. 18, pp. 2792–2794, 2006.

[25] A.-P. Liu *et al.*, "Detecting orbital angular momentum through division-of-amplitude interference with a circular plasmonic lens," *Sci. Rep.*, vol. 3, 2013, Art. no. 2402.

[26] X. Zambrana-Puyalto, X. Vidal, and G. Molina-Terriza, "Angular momentum-induced circular dichroism in non-chiral nanostructures," *Nature Commun.*, vol. 5, 2014, Art. no. 4922.

[27] P. B. Johnson and R. W. Christy, "Optical constants of the noble metals," *Phys. Rev. B*, vol. 6, no. 12, pp. 4370–4379, 1972.

[28] P. Zilio, G. Parisi, D. Garoli, M. Carli, and F. Romanato, "Bilayer holey plasmonic vortex lenses for the far field transmission of pure orbital angular momentum light states," *Opt. Lett.*, vol. 39, no. 16, pp. 4899–4902, 2014.

[29] L.-L. Wang, X.-F. Ren, R. Yang, G.-C. Guo, and G.-P. Guo, "Transmission of doughnut light through a bull's eye structure," *Appl. Phys. Lett.*, vol. 95, no. 11, 2009, Art. no. 111111.

[30] N. Shitrit, I. Bretner, Y. Gorodetski, V. Kleiner, and E. Hasman, "Optical spin hall effects in plasmonic chains," *Nano Lett.*, vol. 11, no. 5, pp. 2038–2042, 2011.

[31] Y. Gorodetski, N. Shitrit, I. Bretner, V. Kleiner, and E. Hasman, "Observation of optical spin symmetry breaking in nanoapertures," *Nano Lett.*, vol. 9, no. 8, pp. 3016–3019, 2009.

[32] R. de Waele, S. P. Burgos, A. Polman, and H. A. Atwater, "Plasmon dispersion in coaxial waveguides from single-cavity optical transmission measurements," *Nano Lett.*, vol. 9, no. 8, pp. 2832–2837, 2009.

[33] M. J. Lockyear, A. P. Hibbins, J. R. Sambles, and C. R. Lawrence, "Microwave transmission through a single subwavelength annular aperture in a metal plate," *Phys. Rev. Lett.*, vol. 94, no. 19, 2005, Art. no. 193902.

[34] P. B. Catrysse and S. Fan, "Understanding the dispersion of coaxial plasmonic structures through a connection with the planar metal-insulator-metal geometry," *Appl. Phys. Lett.*, vol. 94, no. 23, 2009, Art. no. 231111.

[35] A. Niv, G. Biener, V. Kleiner, and E. Hasman, "Manipulation of the Pancharatnam phase in vectorial vortices," *Opt. Exp.*, vol. 14, no. 10, pp. 4208–4220, 2006.

[36] N. Bozinovic *et al.*, "Terabit-scale orbital angular momentum mode division multiplexing in fibers," *Science*, vol. 340, no. 6140, pp. 1545–1548, 2013.

[37] X. Li, T.-H. Lan, C.-H. Tien, and M. Gu, "Three-dimensional orientation-unlimited polarization encryption by a single optically configured vectorial beam," *Nature Commun.*, vol. 3, 2012, Art. no. 998.